Checkpoint Blockade–Induced Dermatitis and Colitis Are Dominated by Tissue-Resident Memory T Cells and Th1/Tc1 Cytokines

Robin Reschke[1], Jason W. Shapiro[2], Jovian Yu[3], Sherin J. Rouhani[3], Daniel J. Olson[3], Yuanyuan Zha[4], and Thomas F. Gajewski[1,3]

ABSTRACT

Immune checkpoint blockade is therapeutically successful for many patients across multiple cancer types. However, immune-related adverse events (irAE) frequently occur and can sometimes be life threatening. It is critical to understand the immunologic mechanisms of irAEs with the goal of finding novel treatment targets. Herein, we report our analysis of tissues from patients with irAE dermatitis using multiparameter immunofluorescence (IF), spatial transcriptomics, and RNA *in situ* hybridization (RISH). Skin psoriasis cases were studied as a comparison, as a known Th17-driven disease, and colitis was investigated as a comparison. IF analysis revealed that $CD4^+$ and $CD8^+$ tissue-resident memory T (T_{RM}) cells were preferentially expanded in the inflamed portion of skin in cutaneous irAEs compared with healthy skin controls. Spatial transcriptomics allowed us to focus on areas containing T_{RM} cells to discern functional phenotype and revealed expression of Th1-associated genes in irAEs, compared with Th17-asociated genes in psoriasis. Expression of PD-1, CTLA-4, LAG-3, and other inhibitory receptors was observed in irAE cases. RISH technology combined with IF confirmed expression of IFNγ, CXCL9, CXCL10, and TNFα in irAE dermatitis, as well as IFNγ within T_{RM} cells specifically. The Th1-skewed phenotype was confirmed in irAE colitis cases compared with healthy colon.

Introduction

Immune checkpoint blockade (ICB) can produce durable clinical responses in patients with various types of cancer. However, such treatment is frequently associated with immune-related adverse events (irAE). Between 25% and 40% of patients develop a cutaneous irAE (cirAE) during ICB, with higher frequencies observed when patients are treated with combination anti–PD-1 + anti–CTLA-4 (1). cirAEs can be clinically divided into various subtypes. Most frequently seen are maculopapular and lichenoid rashes (2), while a minority of patients can exhibit bullous drug eruptions or Sweet's syndrome (3, 4). In most mild cirAE cases, treatment with topical or oral corticosteroids is sufficient to resolve the rash. However, corticosteroids globally suppress T-cell function (5), and it has been reported that high-dose steroids can negatively influence survival of patients with metastatic melanoma (6). Therefore, it is important to understand the biology of immune-related dermatitis better to tailor a more personalized treatment approach.

On the basis of the occurrence of vitiligo upon ICB of patients with melanoma, a condition in which T cells and antibodies reacting to melanoma antigens can cross-react on normal melanocytes leading to skin depigmentation (7), it had been presumed that other irAEs might also be mediated by immune cross-reactivity. However, in contrast to vitiligo which only occurs in patients with melanoma, other irAEs appear to be tumor-type agnostic. Therefore, it is necessary to consider alternative mechanisms by which immune checkpoint inhibitors might promote immune reactions in normal tissues. One hypothesis is that irAEs occur through effects on tissue-resident memory T (T_{RM}) cells, which are retained in tissues after resolution of infection and other immune responses (8). T_{RM} cells are characterized by expression of CD69 and/or CD103, and can be of either the $CD4^+$ or the $CD8^+$ lineage (8). In addition, T_{RM} cells can be of various functional phenotypes, including Th1, Th2, or Th17 (8). Psoriasis has been reported to be a Th17-like disease (9), but the immune phenotype in cirAEs has been unclear. We therefore studied skin biopsies from patients with irAE dermatitis compared with those from patients with psoriasis using immunofluorescence (IF), spatial transcriptomics, and RNA *in situ* hybridization (RISH). Results were extended to irAE colitis cases, to explore whether similar mechanisms were seen in a second affected tissue.

Materials and Methods

Patient samples

This research was performed in accordance with the Declaration of Helsinki. For spatial transcriptomics, RISH, and multiparameter IF staining, we used archived formalin-fixed paraffin-embedded (FFPE) tissue sections from 22 patients with cirAEs (grade 2/3; Supplementary Table S1). Patients with grade 1 irAEs were excluded. In addition, healthy skin samples from ten patients undergoing breast or fat reduction, and skin biopsies from 3 patients with psoriasis were used as controls. None of these patients (cirAE, psoriasis, breast/fat reduction) had received immune suppression. In addition, seven irAE colitis cases (grade 3 /4) and eight healthy colon samples were processed for spatial transcriptomics. One extra irAE colitis case was included for IF and RISH ($n = 8$; Supplementary Table S2). Samples from 2 patients

[1]Department of Pathology, University of Chicago, Chicago, Illinois. [2]Center for Research Informatics, University of Chicago, Chicago, Illinois. [3]Department of Medicine, Section of Hematology/Oncology, University of Chicago, Chicago, Illinois. [4]Human Immunological Monitoring Facility, University of Chicago, Chicago, Illinois.

Corresponding Author: Thomas F. Gajewski, Departments of Pathology and Medicine, University of Chicago, 5841 S. Maryland Avenue, Chicago, IL 60637. Phone: 773-702-4601; Fax: 773-702-3163; E-mail: tgajewski@medicine.bsd.uchicago.edu

Cancer Immunol Res 2022;10:1167–74

doi: 10.1158/2326-6066.CIR-22-0362

with atopic dermatitis were used for optimization of IF staining conditions. FFPE blocks were stored at room temperature until processing. Four of 8 patients with irAE colitis received corticosteroids at the time of the biopsy. All colon biopsies were obtained during diagnostic colonoscopies. Gender was equally distributed (26 male/24 female patients). The study was conducted after approval by the University of Chicago Institutional Review Board (IRB protocol 15-0837) as a component of the immunotherapy biobanking protocol. Informed written consent was obtained from patients before performing biopsies.

Multiparameter IF

A five-color multiplex quantitative IF protocol was developed to detect cell surface markers using antibodies specific for CD3 (Biocare Medical, catalog no. CME 324), CD8 (Novus Bio, catalog no. NBP232836B), CD69 (Abcam, catalog no. Ab233396), CD103 (Biocare Medical, catalog no. ACI3117A), and CD20 (Thermo Fisher Scientific, catalog no. MA5-13141) on FFPE tissue sections. 4′,6-Diamidin-2-phenylindol (DAPI) was used to identify the cells. 5 μmol/L FFPE sections were deparaffinized and the tissues fixed with formaldehyde prior to antigen retrieval. Antigen retrieval was performed using Akoya Bioscience antigen retrieval buffer with low pH (pH 6; catalog no. AR600250ML) or high pH (pH 9; catalog no. AR900250ML). Each section underwent five rounds of antibody staining, each round consisting of blocking (Akoya Bioscience, catalog no. ARD1001EA), primary antibody incubation, horseradish peroxidase–conjugated secondary antibodies (Akoya Bioscience ARH1001EA) incubation, tyramide signal amplification (TSA) visualization with fluorophores Opal 480 (Akoya Bioscience FP1500001KT), Opal 520 (Akoya Bioscience, catalog no. FP1487001KT), Opal 570 (Akoya Bioscience, catalog no. FP1488001KT), Opal 620 (Akoya Bioscience, catalog no. FP1495001KT), and Opal 690 (Akoya Biosciences, catalog no. FP1488001KT) diluted in 1X Plus Amplification Diluent (Akoya Biosciences, catalog no. FP1135), and pressure cooker treatment. Tissue sections were then incubated with DAPI solution (Akoya Bioscience, catalog no. FP1490) for 5 minutes at room temperature and mounted in ProLong Diamond Antifade Mountant (Invitrogen, catalog no. P36961). Scanning of the slides was performed using the Vectra Polaris Imaging Station and Phenochart 1.1.0 software (Akoya Biosciences). Five to 35 representative regions of interest (ROI) for each tissue section were acquired at 20× magnification as multispectral images. A supervised machine learning algorithm within the Inform 2.3 software (Akoya Biosciences), which assigned trained phenotypes and Cartesian coordinates to cells, was used to perform image analysis and cell phenotyping. ROIs were chosen to cover epidermis and subepidermal immune-cell infiltrates. To achieve optimal staining conditions for each marker, we first tested singleplex assays using human atopic dermatitis tissue as an example for inflamed skin tissue. The results from the singleplex assays were used as reference point for antigen visualization. After successful optimization of all markers individually, they were combined into a multiplexed IF panel. Each marker was tested for its ideal condition and position in the sequence of multiplex staining. Markers in multiplex staining were visually compared with the corresponding singleplex staining for intensity and pattern. Using this visual comparison, we were able to find the optimal signal through dilution of the primary antibodies and/or fluorophores to achieve similar results for the single and multiplex IF staining for each antibody (Supplementary Fig. S1). Through optimal sequencing of antibody staining, interference between each antibody was held to a minimum. The number of $CD4^+$ cells was approximated by counting $CD3^+$ cells that were $CD8^-$.

Spatial transcriptomics

We processed 11 FFPE samples (two irAE dermatitis, two psoriasis, and seven irAE colitis) using 10x Genomics Visium FFPE kit (10× Genomics, catalog no. 1000338). Briefly, tissue RNAs were isolated using Allprep DNA/RNA FFPE kit (Qiagen, catalog no. # 80234) and quality controlled (DV200 ≥ 50%). A total of 5 μmol/L tissue sections were cut and placed onto capture areas of the gene expression slides. After drying overnight, slides were dried again for 2 hours at 60°C. Then, they were deparaffinized and covered in hematoxylin (Millipore Sigma, catalog no. MHS16) for 3 minutes at room temperature. After intermittent washing steps, they were covered in Bluing reagent (Agilent, catalog no. CS70203-2) and later Eosin (Millipore Sigma, catalog no. HT110116). Hematoxylin and eosin (H&E)-stained slides were finally imaged on a Nikon T2 Microscope. The spatial transcriptome library was prepared following the manufacturer's instruction and sequenced on the NovaSeq 6000 system at the University of Chicago Genomics core facility. Space Ranger from 10x Genomics (https://support.10xgenomics.com/spatial-gene-expression/software/pipelines/latest/what-is-space-ranger) was used to build the initial count matrices for each unique molecular identifier (UMI) at each location in each sample and create the output files used for downstream analysis in R with Seurat v4. Downstream analysis was done using R packages Seurat and Giotto. Each sample was filtered to remove any barcodes with low counts of either UMIs or genes. For larger tissues with over 1,000 genes per spot, we required at least 500 UMIs and 250 genes per spot, whereas for samples with fewer genes per spot, we relaxed these criteria to 200 UMIs and 100 genes. Filtered data were then normalized using the "sctransform" method to correct for intrasample variation in UMI density (https://github.com/satijalab/sctransform). Using these normalized data, we followed Seurat's guidelines for data integration to control for sample-specific batch effects. The integrated dataset was then clustered based on a set of 3,000 variable features shared across samples, and clusters were annotated manually based on both the histology of the tissue and on the presence of known marker genes for different cell types. Each spot in a Visium dataset corresponds to 1 to 10 cells.

RISH combined with IF staining for protein

Codetection of RNA and protein antigens in the same samples was achieved by RISH using the RNAScope Multiplex Fluorescent Reagent Kit v2 (Advanced Cell Diagnostics, catalog no. 323110), together with antibody-based IF staining. Positive (POLRA2, PPIB, UBC) and negative RNA probe (dapB) controls, *CXCL10* RNA probe (catalog no. 311851), *IFNG* RNA probe (catalog no. 310501-C1/2), *TNF* RNA probe (catalog no. 310421-C1/2), *CXCL9* RNA probe (catalog no. 440161), *IL5* RNA probe (catalog no. 319391), *CD69* RNA probe (catalog no. 494471-C2), and CD45 antibody (Biocare Medical, catalog no. CM016) were tested individually on human atopic dermatitis sections. We had already optimized the CD45 antibody in concert with RNA probes in a previous publication (10). Therefore, optimal signal through dilatation for the primary antibody in singleplex and in the codetection workflow was already known. Nonetheless, we performed staining of the individual targets on human atopic dermatitis first (Supplementary Fig. S1). After successful staining of this comparably inflamed skin tissue, all markers were stained together with the codetection protocol. The manufacturer's integrated codetection protocol was followed. Markers in multiplex staining were visually compared with the corresponding singleplex staininig for intensity and pattern (Supplementary Fig. S1). ROIs for each tissue section were acquired at 40× magnification. ROIs were chosen to cover epidermis and subepidermal leukocytic infiltrates. We have previously described

in detail the Advanced Cell Diagnostics bio Co-detection workflow and downstream analysis (10).

Statistical analysis

Statistics were done using R 4.0.5 (https://www.R-project.org/), and the tidyverse (https://www.tidyverse.org/), patchwork (https://patchwork.data-imaginist.com/), phenoptr (https://akoyabio.github.io/phenoptr/), ggsignif (https://github.com/const-ae/ggsignif), ggpmisc (https://github.com/aphalo/ggpmisc), ggpubr (https://rpkgs.datanovia.com/ggpubr/), giotto (https://rubd.github.io/Giotto_site/), future (ttps://future.futureverse.org/), and scales (https://scales.r-lib.org/) packages. We tested for spatial colocalization of key genes (*CD3E*, *CD4*, *CD8A*, *CD8B*, *CD69*, *ITGA1*, *IFNG*, and *TNF*) by estimating spatial correlations using the R package Giotto. Giotto is a complimentary tool for analyzing spatial transcriptomic data, including functions for spatial deconvolution and estimating correlation and coexpression of specific genes. To estimate correlations across both irAE dermatitis samples and across both psoriasis samples, we first exported the filtered count data from a merged Seurat object and then created a merged Giotto object (one for irAE dermatitis and one for psoriasis) by concatenating the count data and combining the spatial location data for each sample, using an offset for the *y* coordinates to keep the samples from overlapping. We then followed a standard Giotto workflow to reprocess the counts, including normalization with the *normalizeGiotto* function, dimension reduction with *runPCA*, UMAP with *runUMAP* and clustering with *createNearestNetwork* and *doLeidenCluster*. Finally, the data were converted to a network representation using *createSpatialNetwork* and spatial correlations of the above genes were estimated with *detectSpatialCorGenes* (https://rubd.github.io/Giotto_site/). This function averages spatial expression by accounting for the network topology and then estimates Pearson correlations. We exported the smoothed expression data used in this step to also estimate *P* values using the complementary function *cor.test* from base R. Results were then visualized with the package corrplot

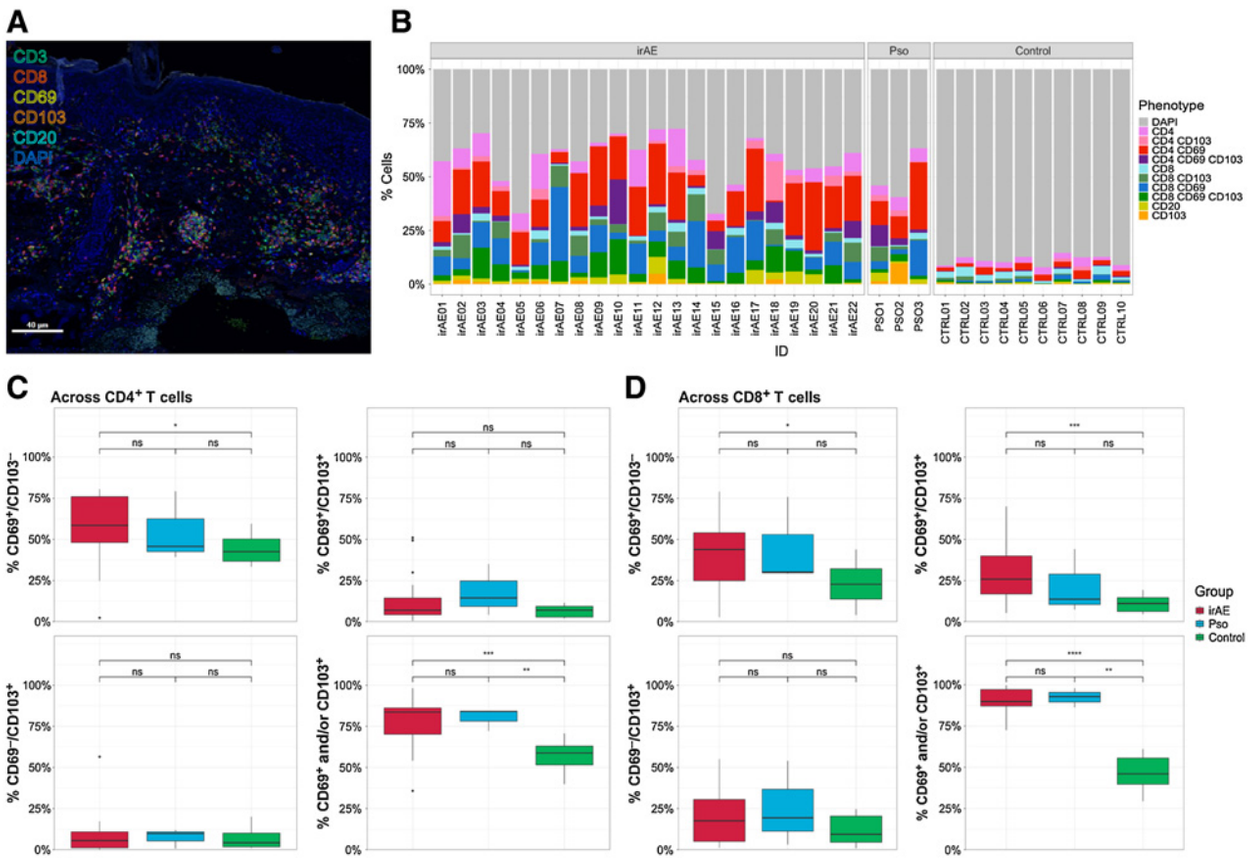

Figure 1.

irAE dermatitis presents with expanded T_{RM} cells compared with healthy controls. **A,** Multiplex IF staining of a representative irAE dermatitis sample with CD3 (green), CD8 (red), CD69 (yellow), CD103 (orange), CD20 (turquoise), and DAPI (blue). The sample is representative of 22 cirAE samples. **B,** Cell proportions across all 22 irAE dermatitis samples, three psoriasis (pso) samples and 10 (healthy) controls on a per patient basis: Percentages of $CD4^+$ cells (pink), $CD4^+CD103^+$ cells (rose), $CD4^+CD69^+$ cells (red), $CD4^+CD69^+CD103^+$ cells (purple), $CD8^+$ cells (turquoise), $CD8^+CD103^+$ cells (light green), $CD8^+CD69^+$ cells (blue), $CD8^+CD69^+CD103^+$ cells (dark green), $CD20^+$ cells (yellow), $CD103^+$ (orange), and DAPI (light gray). **C,** Percentage of all $CD4^+$ T_{RM}-cell phenotypes alone and combined (either $CD69^+$ or $CD103^+$ single positive or $CD69^+CD103^+$ double positive $CD4^+$ cells) of all cells correlated with skin pathology group: irAE versus pso versus healthy. **D,** Percentage of all $CD8^+$ T_{RM}-cell phenotypes alone or combined of all $CD8^+$ cells correlated with skin pathology group: irAE versus pso versus healthy. Comparisons were performed using a Wilcoxon rank-sum test, *P*-value ranges: ****, $P \leq 0.0001$ "***" as < 0.001, "**" as < 0.01, "*" as < 0.05, and "ns" indicating not significant. The middle line represents the median, top/bottom of the box represent 25th/75th percentile and the whiskers represent the largest/smallest value under 1.5 × interquartile range, with further points denoted individually as outliers.

using significance levels of 0.001, 0.01, and 0.05. Signatures were estimated on the basis of chemokines (*CXCL9*, *CXCL10*, *CXCL11*), IFN-induced genes (HLA-DR, *CD74*, *GBP5*), and inhibitory checkpoint genes (*PDCD1*, *CTLA4*, *HAVCR2*, *TIGIT*, *LAG3)* using the package UCell applied to expression values normalized by the aggregate of *CD3D*, *CD3E*, and *CD3G* in each spot. UCell corrects for compositional differences between cells by using a Mann–Whitney test statistic to estimate signature scores (11).

Data availability

The processed count data and metadata for the samples analyzed for spatial transcriptomics are available through Gene Expression Omnibus under accession GSE210037. The BioProject number for the raw sequence data is PRJNA863563. All analysis scripts are available from the corresponding author upon reasonable request. All other data generated in this study are available within the article and its Supplementary Data or from the corresponding author upon reasonable request.

Ethics approval

IRB protocol 15-0837.

Results

To enhance understanding of irAE dermatitis, we examined FFPE skin biopsy specimens from affected patients. Our hypothesis was that irAE dermatitis might be characterized by reactivated T_{RM} cells, with either a Th1-, Th2-, or Th17-like phenotype. As a first approach, we stained cirAE tissue from 22 patients (Supplementary Table S1) with an IF 5-plex panel that contained the T_{RM} markers CD69 and CD103 along with CD4, CD8, and CD20 (**Fig. 1A** and **B**; Supplementary Figs. S2 and S3). In addition to staining skin samples from 10 healthy controls, we used three psoriasis specimens as a comparison group because this autoimmune skin disease has been reported to be triggered by T_{RM} cells and is known to have a Th17-dominant T-cell infiltration (9, 12). The percentage of B cells and CD103 single positive cells was higher in the irAE samples compared with healthy controls ($P \le 0.01$ and $P \le 0.05$; Supplementary Fig. S4). In addition, we found a significant expansion of $CD8^+$ and $CD4^+$ T_{RM} cells in the 22 irAE cases, and also in psoriasis (Supplementary Fig. S4). Between 70% and 90% of all $CD4^+$ and $CD8^+$ T cells exhibited at least one feature of tissue residency (expression of either CD69 or CD103 alone or both) in the patients with cirAE (**Fig. 1C** and **D**). In contrast, in the healthy controls, only 40% to 65% of $CD4^+$ and $CD8^+$ T cells stained positive

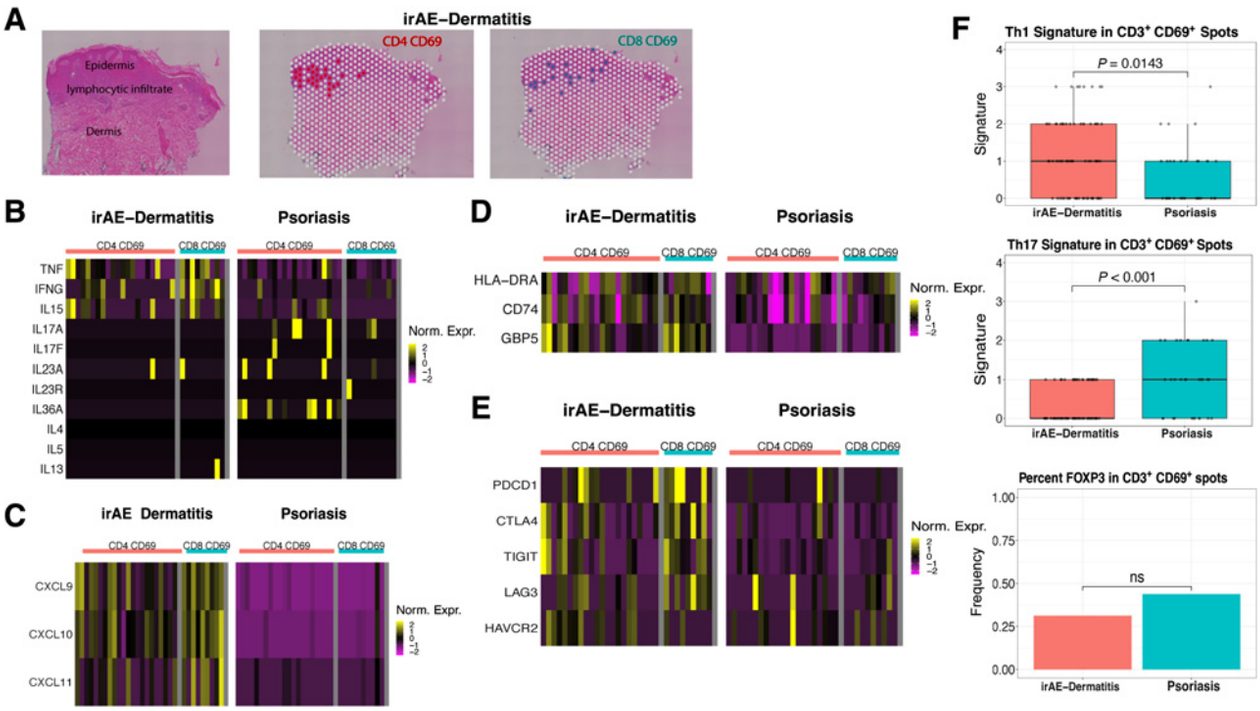

Figure 2.

irAE dermatitis is characterized by Th1/Tc1 T_{RM} cells with upregulated inhibitory checkpoint molecules. Spatial transcriptomic analysis was performed on two irAE dermatitis and two psoriasis samples. **A,** One irAE dermatitis H&E stain: Irregular acanthotic epidermis, hyperkeratosis and dense lymphocytic infiltrate. Coexpression spatial plot with red spots for $CD4^+CD69^+$ coexpression and turquoise/blue spots for $CD8^+CD69^+$ coexpression in one irAE dermatitis case. **B,** Heat map showing cytokine expression. **C,** Heat map showing expression of chemokines. **D,** Heat map showing expression of IFN-induced genes. **E,** Heat map showing expression of inhibitory checkpoint molecules. Only spots uniquely expressing either $CD4^+CD69^+$ or $CD8^+CD69^+$ shown in the heat maps. **F,** Th1/Th17 scores equal to the number of Th1/Th17 signature genes appearing at least once in each spot. Th1 signature consisting of *IFNG*, *TBX21*, and *STAT4* genes expressed in $CD3^+CD69^+$ spots. Th17 signature consisting of *RORC*, *IL17A/F*, *IL23A/R*, and *IL36A* genes expressed in $CD3^+CD69^+$ spots. Percentage of $CD3^+CD69^+$ spots expressing *FOXP3*. We estimated the distribution of Th1 and Th17 scores across all $CD3^+CD69^+$ spots in each sample and evaluated significance using the nonparametric two-sample Wilcoxon test. The middle line represents the median, top/bottom of the box represent 25th/75th percentile and the whiskers represent the largest/smallest value under 1.5 × interquartile range, black dots showing distribution of all data points, "ns" means not significant.

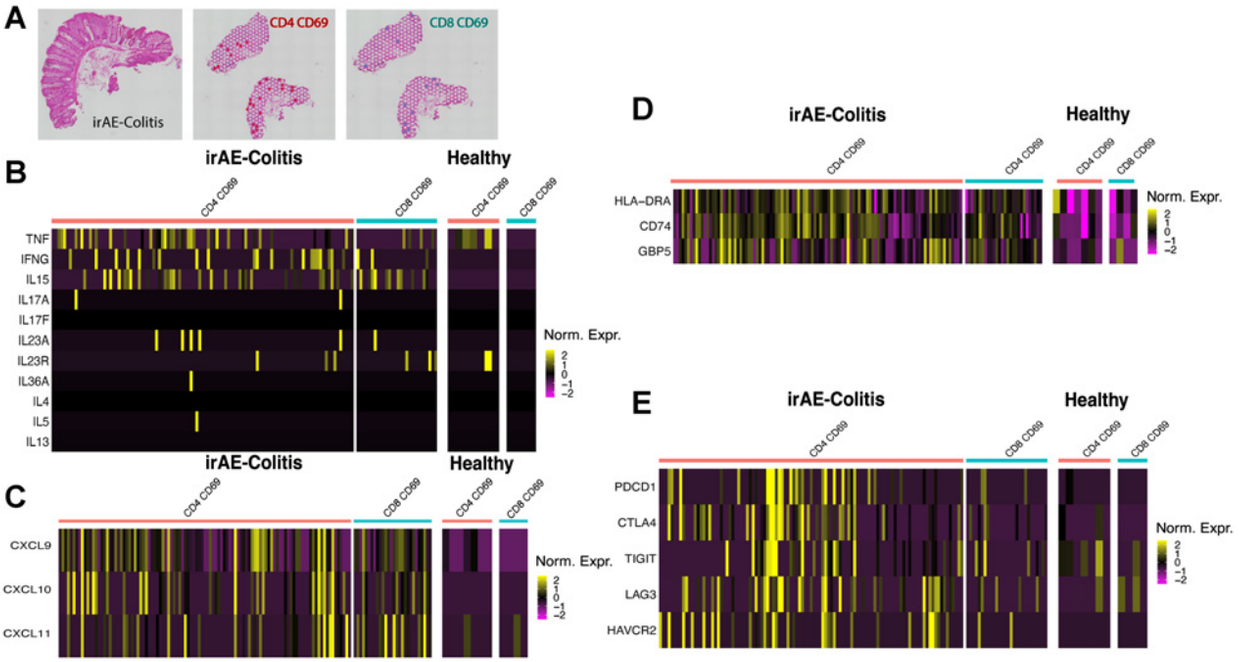

Figure 3.

irAE colitis is characterized by Th1/Tc1 T_{RM} cells and upregulated inhibitory checkpoint molecules. Spatial transcriptomic analysis was performed on seven irAE colitis and eight healthy colon samples. **A,** H&E stain of an exemplary irAE colitis case showing an extensive lymphocytic infiltrate below epithelial crypts. Coexpression spatial plot with red spots for $CD4^+CD69^+$ coexpression and turquoise spots for $CD8^+CD69^+$ coexpression in irAE colitis. **B,** Heat map showing cytokine expression. **C,** Heat map showing chemokine expression. **D,** Heat map showing expression of IFN-induced genes. **E,** Heat map showing expression of genes encoding inhibitory checkpoint molecules. Only spots uniquely expressing either $CD4^+CD69^+$ or $CD8^+CD69^+$ are shown in the heat maps.

for T_{RM} cell markers ($P \leq 0.001$ and $P \leq 0.0001$). We conclude that irAE dermatitis is dominated by expansion of T_{RM} cells.

To determine the transcriptional profile of areas (spots) containing T_{RM} cells in irAE dermatitis, we employed spatial transcriptomic technology on two cirAE and two psoriasis samples. H&E-stained tissue was utilized to provide information about tissue architecture. Sections were visually divided into epidermis, a subepidermal lymphocyte cluster, and dermis (**Fig. 2A**). We were able to visualize cell clusters from irAE and psoriasis samples two-dimensionally (Supplementary Fig. S5). We observed that irAE and psoriasis samples shared a common spatial and cellular make-up with five major cellular clusters. Clusters 0, 1, and 5 represented immune cells, predominantly consisting of lymphocytes subepidermally. Cluster 2 contained the epidermis with keratinocytes. Clusters 3 and 4 were represented by fibroblasts and dead keratinocytes (stratum corneum). A similar distribution of clusters was seen for irAE and psoriasis samples. However, obvious differences were found when examining the transcriptional profile corresponding to areas with CD4/CD8 and CD69 coexpression. The cytokine genes *TNFA*, *IFNG*, and *IL15* were more abundantly expressed in irAEs (**Fig. 2B**), whereas *IL17A*, *IL17F*, *IL23A*, *IL23R*, and *IL36A* were predominantly seen in psoriasis (**Fig. 2B**). We did not see marked Th2 cytokine expression. *IL4* and *IL5* were not expressed at all and *IL13* only rarely in the $CD8^+CD69^+$ spots. IFNγ–induced genes such as HLA-DRA, *CD74*, and *GBP5* as well as the chemokines *CXCL9*, *CXCL10*, and *CXCL11*, were expressed at significantly higher levels in irAE samples than in psoriasis ($P < 0.001$; **Fig. 2C** and **D**; Supplementary Fig. S6). CXCL9/10/11 can recruit effector T cells by engaging the CXCR3 receptor. High expression of the genes encoding inhibitory T-cell checkpoint molecules PD-1, CTLA-4, LAG-3, TIM3, and TIGIT was detected in cirAEs and rarely seen in psoriasis (**Fig. 2E**). When we comprised a signature for inhibitory checkpoints and normalized for CD3 expression (*CD3G*, *CD3D*, *CD3E*) we saw significantly more expression in our cirAE samples ($P < 0.001$; Supplementary Fig. S6). We designed a Th1 score consisting of *IFNG*, *TBX21*, and *STAT4* and showed that significantly more $CD3^+CD69^+$ spots in irAE samples expressed these signature genes than in psoriasis (**Fig. 2F**), suggesting that Th1/Tc1 cells are the dominant-cell phenotype in irAEs (13). Conversely, a Th17 score of the Th17-related genes *RORC*, *IL17A*, *IL17F*, *IL36A*, *IL23A*, and *IL23R* was significantly higher in psoriasis (**Fig. 2F**). The gene encoding the transcription factor for regulatory T cells FoxP3 was expressed similarly in the $CD3^+CD69^+$ regions of cirAEs and psoriasis (**Fig. 2F**). Overall, these data suggest that irAE dermatitis is characterized by a Th1/Tc1-centered immune response.

Leveraging spatial transcriptomics, we examined an independent cohort of seven irAE colitis cases. In **Fig. 3A**, we show H&E-stained irAE colitis and the spatial distribution of T_{RM} cells ($CD4/CD8^+$ $CD69^+$ spots) in a representative image. These cases also showed an upregulation of cytokines and chemokines correlating with a Th1/Tc1 response, including *IFNG*, *TNFA*, *CXCL9*, *CXCL10*, and *CXCL11* (**Fig. 3B** and **C**). Similarly, an upregulation of IFN-induced genes and checkpoint molecules was observed (**Fig. 3D** and **E**). Expression of IL15, which T_{RM} cells require IL15 for their differentiation and survival (12), was seen across irAE cases (both skin and colon; **Figs. 2B** and **3B**). We compared results with eight healthy colon samples and found that Th1/Tc1 cytokines, CXCL9-11, IFN-induced genes, and checkpoint molecules were more dominantly expressed in irAE colitis than in healthy colon samples (**Fig. 3B–E**).

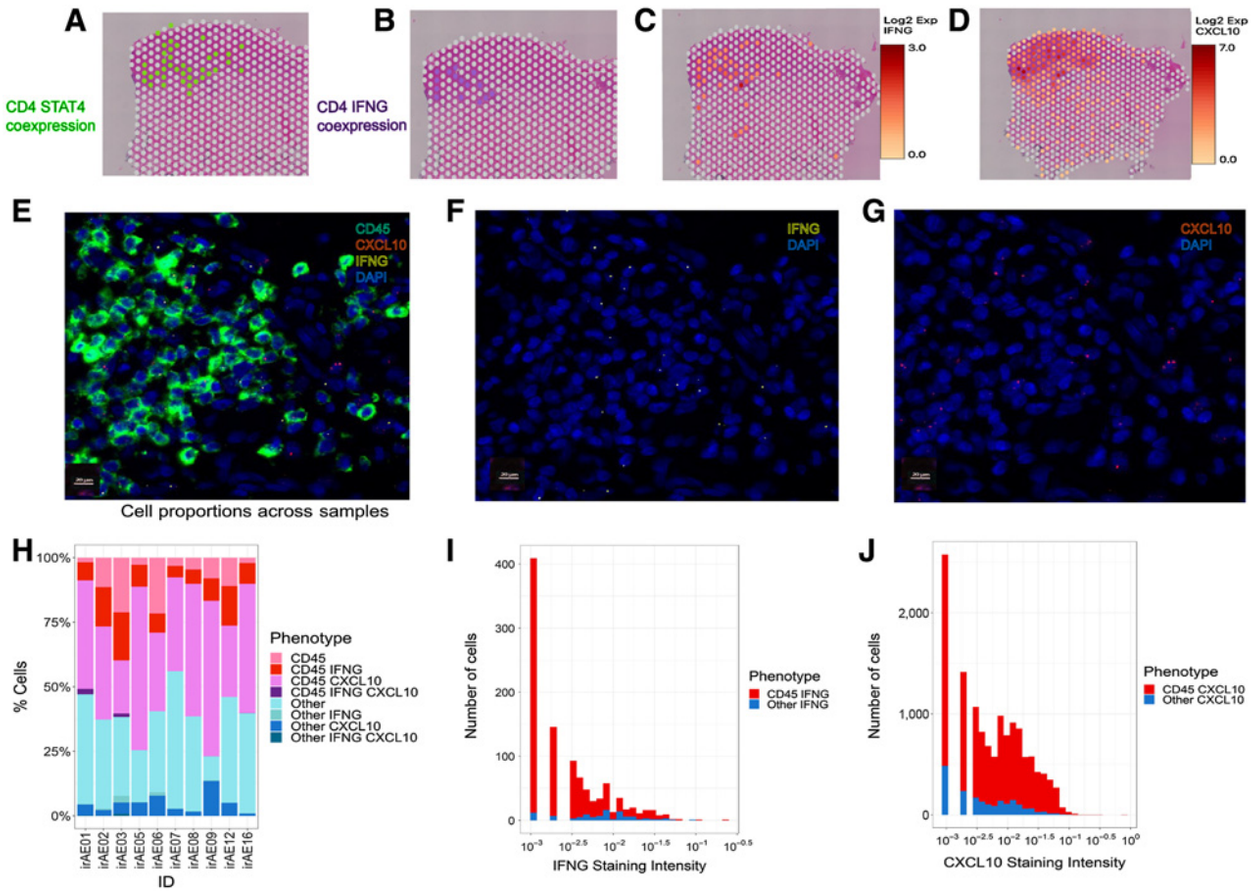

Figure 4.

irAE dermatitis presents with Th1-oriented transcripts. **A–D,** Spatial transcriptomic analysis detected coexpression of CD4, *STAT4*, and *IFNG*, and showed spatial distribution of *IFNG* and *CXCL10* expression levels, Shown in **A–D** are plots showing one representative of two samples. **E–H,** Combined IF-RISH analysis showed colocalization of CD45 with *CXCL10* and *IFNG* in 10 samples. Representative images of one of 10 analyzed cases are shown. **A,** Plot showing *CD4* and *STAT4* coexpression with green spots in one irAE dermatitis case **B,** Plot showing coexpression of *CD4* and *IFNG* with purple spots in one irAE dermatitis case. **C,** Spatially distributed expression levels of *IFNG* across one irAE sample. **D,** Spatially distributed expression levels of *CXCL10* across one irAE sample. **E,** ROI of the complete IF–RISH panel consisting of $CD45^+$ cells (green), *CXCL10* transcripts (red), *IFNG* transcripts (yellow spots), DAPI (blue). **F,** Only *IFNG* (yellow), and DAPI (blue) shown, one yellow dot represents one transcript. **G,** Only *CXCL10* (red), and DAPI (blue) shown, one red dot represents one transcript. **H,** Distribution of cell phenotypes (percentage of cells) across 10 cirAE cases. Phenotypes are $CD45^+$, $CD45^+IFNG^+$, $CD45^+CXCL10^+$, $CD45^+IFNG^+CXCL10^+$, $Other^+$, $Other^+IFNG^+$, $Other^+CXCL10^+$ and $Other^+IFNG^+CXCL10^+$ cells. **I,** Histogram showing staining intensity of *IFNG* within $CD45^+$ cells (red) or $Other^+$ (CD45 neg.) cells (blue). **J** Histogram showing staining intensity of *CXCL10* within $CD45^+$ cells (red) and $Other^+$ (CD45 neg.) cells (blue). $IFNG^+$ cells and $CXCL10^+$ cells measured by mean fluorescence intensity (on a per cell basis).

The most upregulated adhesion molecule in irAE dermatitis and also irAE colitis was ITGA4 (Supplementary Fig. S5), which was almost not expressed in psoriasis and less frequently seen in healthy colon.

We observed colocalization of spots containing expression of *STAT4*, *IFNG*, and CD4 (**Fig. 4A** and **B**) and a strong correlation between expression of *CD3E* or *CD69* and *IFNG* ($P < 0.001$; Supplementary Fig. S5) but the spatial transcriptomic procedure was technically challenging with skin tissue. To confirm transcriptomic data on a larger number of skin samples, we utilized RISH for key Th1/Tc1-associated transcripts on 10 independent cirAE cases. This analysis confirmed strong expression of *IFNG* and *CXCL10* (**Fig. 4C–G**), which was largely found among $CD45^+$ cells (**Fig. 4H–J**). However, other nuclei staining with DAPI but not CD45 also showed expression of *CXCL10* (**Fig. 4H** and **J**), suggesting that fibroblasts and/or keratinocytes may additionally produce this chemokine in response to locally secreted IFNγ. Similarly, *CXCL9* was mainly found within $CD45^+$ cells but also to a lesser extent in $CD45^-$ cells (Supplementary Fig. S7). In addition, we stained for *TNFA* transcripts, which localized predominantly within $CD45^+$ cells (Supplementary Fig. S7). This pattern is also reflected by the stronger fluorescence intensity of *TNFA* and *CXCL9* mRNA within $CD45^+$ cells (Supplementary Fig. S7). The same pattern was also reflected in eight irAE colitis cases (Supplementary Fig. S8). Most of the expression of TNFA and CXCL9 was seen within $CD45^+$ cells (Supplementary Fig. S8). However, epithelial cells also produced *CXCL9*. This corresponds with the spatial information from the spatial transcriptomic analysis (Supplementary Fig. S8).

To clarify whether T_{RM} cells were producing key cytokines, we used two more IF–RISH panels and found that $CD69^+CD3^+$ cells were producing the majority of *IFNG* in irAE dermatitis (Supplementary Fig. S9). Despite technical issues with spatial transcriptomics of our

two bullous irAE cases, we interrogated the possibility of Th2 cytokine production in bullous irAEs by using combined IF–RISH. We found some expression of *IL5* within $CD69^+CD3^+$ cells, arguing for a mixed Th1/Th2 response in bullous irAEs (Supplementary Fig. S10). However, *IFNG* expression seemed dominant (**Fig. 4H**). Together, these results confirm a Th1/Tc1-dominant immune reaction in irAE samples.

Discussion

We found evidence that *in situ* expansion of T_{RM} cells with a Th1/Tc1-type cytokine profile was associated with immune-related dermatitis and colitis in patients treated with ICB. A recent study of irAE colitis also identified IFNγ-producing $CD8^+$ T_{RM} cells as associated with immune pathology (14). It is likely that checkpoint-targeting antibodies expand T_{RM} cells as these cells express high levels of the checkpoints constitutively. We observed high expression of CTLA-4, PD1, TIGIT, and LAG3 in cirAEs. T_{RM} cells were the dominant source of *IFNG*, and spots containing these cells also expressed *STAT4* and *TBET*. IFNγ secreted by T cells can stimulate CXCL9/10/11 production by myeloid cells, fibroblasts, and keratinocytes (15, 16) leading to a feed-forward loop amplifying Th1/Tc1 immunity (15). *CXCL9*, *CXCL10*, and *CXCL11* transcripts were abundantly present in cirAE cases and not in psoriasis. Another molecule that was only expressed in irAEs was ITGA4, an adhesion molecule known for homing of Th1 cells into inflamed tissues (17). There is recent evidence indicating that circulating T_{RM} precursor cells can be drawn into inflamed tissues (18). Circulating memory and activated $CD4^+$ T cells have been implicated to precede the occurrence of irAEs independent of affected organs (19, 20). In our cohort, it remains uncertain whether ITGA4- or CXCR3-dependent recruitment of Th1/Tc1 cells contributes to the expansion of the Th1-like T_{RM} compartment through recruitment of circulating T_{RM} precursor cells. However, antibodies targeting ITGA4 such as natalizumab (anti-ITGA4) or vedolizumab (anti-ITGA4+ITGB7) have been demonstrated to have clinical efficacy for ICB-induced meningoencephalomyelitis and steroid-refractory colitis (21, 22). Our data support the notion that existing T_{RM} cell pools with upregulated inhibitory checkpoint molecules expand during ICB. One additional factor that might be shaping the T_{RM} cell pool primarily is microbial antigen presentation, which is particularly important in barrier organs such as skin and intestine. In a mouse model, novel commensals in combination with ICB triggered a T cell–mediated irAE dermatitis, with the vast majority of the bacteria-specific T cells being T_{RM} cells (23).

In contrast to the irAE samples, psoriasis showed stronger expression of Th17-related genes (24, 25). We observed some minor expression of *IL5* in T_{RM} cells of bullous irAE dermatitis. However, investigation of larger numbers of the rarer subtypes of irAEs will be needed to evaluate the prevalence of a mixed Th1/Th2 response. We also cannot completely exclude that there is some involvement of Th17 cells, in particular in patients with psoriasiform cirAEs (26), or that preexisting psoriasis is exacerbated by ICB. Nonetheless, we observed a Th1/Tc1 T_{RM}-cell inflammation with dominant IFNγ production across different cirAEs (lichenoid, maculopapular, bullous) as well as in irAE colitis. Other factors, such as genetic predisposition to specific autoimmune conditions, also might become relevant in determining the ultimate immune phenotype of cirAEs. The Th1/Tc1 T_{RM}-cell inflammation was seen in both patients treated with either anti-PD-1 monotherapy and those treated with anti–PD-1 + anti–CLTA-4 combination therapy.

New targeted approaches of treating irAEs are desirable to avoid systemic immune suppression that may impair antitumoral effector T cells. In irAE microscopic colitis, treatment with a glucocorticoid with low systemic absorption called budesonide has achieved resolution (27). We found that *TNFA* was modestly upregulated in psoriasis but quite strongly expressed in cirAEs. TNFα has been reported to downregulate the sphingosine 1-phosphate receptor 1 (S1PR1) and induce CD69 expression on T cells (28), suggesting a key functional role in generating a tissue-resident state. TNFα can be produced by Th1 cells and by activated macrophages (29, 30). The anti-TNF infliximab has already established efficacy in the treatment of corticosteroid-refractory irAE colitis (31, 32). Furthermore, blocking TNFα preclinically has been shown to augment antitumor immunity in melanoma (33). A clinical study in which infliximab was combined with anti–PD-1 revealed that the efficacy of ICB was preserved (34). Systemic TNFα blockade with infliximab could become relevant for severe steroid-refractory irAE dermatitis. Topical calcineurin inhibitors could target TNFα topically in less severe cases. This treatment has shown efficacy in cutaneous GVHD (35). The dominant Th1/Tc1 T_{RM}-cell axis also suggests the notion of topical therapy with JAK inhibitors should be investigated prospectively.

Authors' Disclosures

R. Reschke reports grants from German Research Foundation (DFG RE 4468/1–1) during the conduct of the study. J. Yu reports personal fees from AbbVie outside the submitted work. S.J. Rouhani reports grants from NIH during the conduct of the study. D.J. Olson reports personal fees from Novartis and grants from American Cancer Society outside the submitted work. T.F. Gajewski reports personal fees from Merck, Jounce, FogPharma, Adaptimmune, Pyxis, Allogene, Catalym, Bicara, Maia, and Samyang outside the submitted work; in addition, T.F. Gajewski has a patent for Evelo licensed, a patent for BMS pending, and a patent for Pyxis licensed; and cofounder/shareholder: Jounce and Pyxis Oncology. No disclosures were reported by the other authors.

Authors' Contributions

R. Reschke: Conceptualization, data curation, formal analysis, validation, investigation, visualization, methodology, writing–original draft, project administration, writing–review and editing. **J.W. Shapiro:** Data curation, software, formal analysis, visualization. **J. Yu:** Data curation, software, visualization. **S.J. Rouhani:** Conceptualization. **D.J. Olson:** Project administration. **Y. Zha:** Methodology. **T.F. Gajewski:** Conceptualization, resources, supervision, funding acquisition, writing–review and editing.

Acknowledgments

We are thankful to Dr. Ernst Lengyel and Malu Zandbergen for providing the Nikon Microscope and Terri Li, Xin Jiang, and Deirdre Anderson from the Human Tissue Resource Center (HTRC).

This work was supported by R35CA210098 from the NCI (TFG).

R. Reschke was funded by the German Research foundation (DFG RE 4468/1-1), J. Yuand S.J. Rouhani were funded by National Institutes of Health Basic Research Training in Medical Oncology grant (T32 CA009566-33).

Note

Supplementary data for this article are available at Cancer Immunology Research Online (http://cancerimmunolres.aacrjournals.org/).

Received May 4, 2022; revised July 22, 2022; accepted August 15, 2022; published first August 17, 2022.

References

1. Larkin J, Hodi FS, Wolchok JD. Combined nivolumab and ipilimumab or monotherapy in untreated melanoma. N Engl J Med 2015;373:1270–1.
2. Coleman E, Ko C, Dai F, Tomayko MM, Kluger H, Leventhal JS. Inflammatory eruptions associated with immune checkpoint inhibitor therapy: a single-institutional, retrospective analysis with stratification of reactions by toxicity and implications for management. J Am Acad Dermatol 2019;80: 990–7.
3. Reschke R, Mockenhaupt M, Simon JC, Ziemer M. Severe bullous skin eruptions on checkpoint inhibitor therapy – in most cases severe bullous lichenoid drug eruptions. J Dtsch Dermatol Ges 2019;17:942–8.
4. Pintova S, Sidhu H, Friedlander PA, Holcombe RF. Sweet's syndrome in a patient with metastatic melanoma after ipilimumab therapy. Melanoma Res 2013;23: 498–501.
5. Libert C, Dejager L. How steroids steer T cells. Cell Rep 2014;7:938–9.
6. Faje AT, Lawrence D, Flaherty K, Freedman C, Fadden R, Rubin K, et al. High-dose glucocorticoids for the treatment of ipilimumab-induced hypophysitis is associated with reduced survival in patients with melanoma. Cancer 2018;124: 3706–14.
7. Lommerts JE, Bekkenk MW, Luiten RM. Vitiligo induced by immune checkpoint inhibitors in melanoma patients: an expert opinion. Expert Opin Drug Saf 2021; 20:883–8.
8. Schreiner D, King CG. CD4+ memory T cells at home in the tissue: mechanisms for health and disease. Front Immunol 2018;9:2394.
9. Marinoni B, Ceribelli A, Massarotti MS, Selmi C. The Th17 axis in psoriatic disease: pathogenetic and therapeutic implications. Auto Immun Highlights 2014;5:9–19.
10. Reschke R, Yu J, Flood BA, Higgs EF, Hatogai K, Gajewski TF. Immune cell and tumor cell-derived CXCL10 is indicative of immunotherapy response in metastatic melanoma. J Immunother Cancer 2021;9:e003521.
11. Andreatta M, Carmona SJ. UCell: Robust and scalable single-cell gene signature scoring. Comput Struct Biotechnol J 2021;19:3796–8.
12. Ryan GE, Harris JE, Richmond JM. Resident memory T cells in autoimmune skin diseases. Front Immunol 2021;12:652191.
13. Murphy KM, Reiner SL. The lineage decisions of helper T cells. Nat Rev Immunol 2002;2:933–44.
14. Sasson SC, Slevin SM, Cheung VTF, Nassiri I, Olsson-Brown A, Fryer E, et al. Interferon-gamma–producing CD8+ tissue resident memory T cells are a targetable hallmark of immune checkpoint inhibitor–colitis. Gastroenterology 2021;161:1229–44.
15. Tokunaga R, Zhang W, Naseem M, Puccini A, Berger MD, Soni S, et al. CXCL9, CXCL10, CXCL11/CXCR3 axis for immune activation – a target for novel cancer therapy. Cancer Treat Rev 2018;63:40–7.
16. Richmond JM, Bangari DS, Essien KI, Currimbhoy SD, Groom JR, Pandya AG, et al. Keratinocyte-derived chemokines orchestrate T-cell positioning in the epidermis during vitiligo and may serve as biomarkers of disease. J Invest Dermatol 2017;137:350–8.
17. Glatigny S, Duhen R, Arbelaez C, Kumari S, Bettelli E. Integrin alpha L controls the homing of regulatory T cells during CNS autoimmunity in the absence of integrin alpha 4. Sci Rep 2015;5:7834.
18. Kok L, Masopust D, Schumacher TN. The precursors of CD8+ tissue resident memory T cells: from lymphoid organs to infected tissues. Nat Rev Immunol 2022;22:283–93.
19. Reschke R, Gussek P, Boldt A, Sack U, Köhl U, Lordick F, et al. Distinct immune signatures indicative of treatment response and immune-related adverse events in melanoma patients under immune checkpoint inhibitor therapy. Int J Mol Sci 2021;22:8017.
20. Lozano AX, Chaudhuri AA, Nene A, Bacchiocchi A, Earland N, Vesely MD, et al. T cell characteristics associated with toxicity to immune checkpoint blockade in patients with melanoma. Nat Med 2022;28:353–62.
21. Abu-Sbeih H, Ali FS, Alsaadi D, Jennings J, Luo W, Gong Z, et al. Outcomes of vedolizumab therapy in patients with immune checkpoint inhibitor–induced colitis: a multi-center study. J Immunother Cancer 2018; 6:142.
22. Basin S, Perrin J, Michot JM, Lambotte O, Cauquil C. Severe anti-PD1-related meningoencephalomyelitis successfully treated with anti-integrin alpha4 therapy. Eur J Cancer 2021;145:230–3.
23. Hu ZI, Link VM, Lima-Junior DS, Delaleu J, Bouladoux N, Han S-J, et al. Immune checkpoint inhibitors unleash pathogenic immune responses against the microbiota. Available from: http://www.pnas.org/doi/10.1073/pnas.2200348119.
24. Harper EG, Guo C, Rizzo H, Lillis JV, Kurtz SE, Skorcheva I, et al. Th17 cytokines stimulate CCL20 expression in keratinocytes *in vitro* and *in vivo*: implications for psoriasis pathogenesis. J Invest Dermatol 2009;129:2175–83.
25. Butcher MJ, Wu CI, Waseem T, Galkina EV. CXCR6 regulates the recruitment of pro-inflammatory IL-17A-producing T cells into atherosclerotic aortas. Int Immunol 2016;28:255–61.
26. Johnson D, Patel AB, Uemura MI, Trinh VA, Jackson N, Zobniw CM, et al. IL17A blockade successfully treated psoriasiform dermatologic toxicity from immunotherapy. Cancer Immunol Res 2019;7:860–5.
27. Hughes MS, Molina GE, Chen ST, Zheng H, Deshpande V, Fadden R, et al. Budesonide treatment for microscopic colitis from immune checkpoint inhibitors. J Immunother Cancer 2019;7:292.
28. Skon CN, Lee JY, Anderson KG, Masopust D, Hogquist KA, Jameson SC. Transcriptional downregulation of S1pr1 is required for establishment of resident memory CD8+ T cells. Nat Immunol 2013;14:1285–93.
29. Kisuya J, Chemtai A, Raballah E, Keter A, Ouma C. The diagnostic accuracy of Th1 (IFN-γ, TNF-α, and IL-2) and Th2 (IL-4, IL-6 and IL-10) cytokines response in AFB microscopy smear negative PTB- HIV co-infected patients. Sci Rep 2019;9:2966.
30. Parameswaran N, Patial S. Tumor necrosis factor-α signaling in macrophages. Crit Rev Eukaryot Gene Expr 2010;20:87–103.
31. Soularue E, Lepage P, Colombel JF, Coutzac C, Faleck D, Marthey L, et al. Enterocolitis due to immune checkpoint inhibitors: a systematic review. Gut 2018;67:2056–67.
32. Johnson DH, Zobniw CM, Trinh VA, Ma J, Bassett RL, Abdel-Wahab N, et al. Infliximab associated with faster symptom resolution compared with corticosteroids alone for the management of immune-related enterocolitis. J Immunother Cancer 2018;6:103.
33. Bertrand F, Rochotte J, Colacios C, Montfort A, Tilkin-Mariamé AF, Touriol C, et al. Blocking tumor necrosis factor α enhances CD8 T-cell-dependent immunity in experimental melanoma. Cancer Res 2015;75:2619–28.
34. Montfort A, Filleron T, Virazels M, Dufau C, Milhès J, Pagès C, et al. Combining nivolumab and ipilimumab with infliximab or certolizumab in patients with advanced melanoma: first results of a phase Ib clinical trial. Clin Cancer Res 2021; 27:1037–47.
35. Elad S, Or R, Resnick I, Shapira MY, Elad S. Topical tacrolimus—a novel treatment alternative for cutaneous chronic graft-versus-host disease. Transpl Int 2003;16:665–70.